J Solid State Electrochem
DOI 10.1007/s10008-013-2271-4

ORIGINAL PAPER

Supercapacitor carbon electrodes with high capacitance

Y. M. Volfkovich · D. A. Bograchev · A. A. Mikhalin · V. S. Bagotsky

Received: 30 May 2013 / Revised: 20 September 2013 / Accepted: 23 September 2013

Abstract Electrochemical behavior of electrodes on the basis of CH900-20 activated carbon (AC) cloth has been studied in concentrated sulfuric acid solution. Cyclic voltammetric curves have been studied in the reversibility range (from 0.1 to 0.9 V RHE) and in the deep cathodic charging potential range (from –0.8 to 1 V RHE). It has been shown that electric double layer (EDL) charging occurs in the reversibility range, while faradaic processes of hydrogen intercalation into AC carbon take place in the range of negative potentials (←0.1 V). The intercalation process is governed by slow solid-phase hydrogen diffusion. The specific charge value grows at an increase in concentrated sulfuric acid solution. The mechanism of double intercalation of sulfuric acid and hydrogen into the AC material is suggested. On the basis of the reached specific discharge capacitance of 1,560 C/g (or 1,110 F/g) and Faraday's law, it has been concluded that the compound of C_6H is formed in the limiting case of deepest cathodic charging. The obtained data have been used in a mathematical charge–discharge model for an AC electrode taking into account the EDL charging and the hydrogen intercalation. The galvanostatic recharge curves have been calculated in the diapason of currents by the developed model.

Keywords Activated carbon · Hydrogen intercalation · Method of standard contact porosimetry · Pseudocapacitance · Solid-phase diffusion · C_6H

Introduction

During the last decades, different new capacitor types were developed based on electrochemical processes. According to Conway [1], an electrochemical capacitor is a device in which different quasi-reversible electrochemical charge–discharge processes take place and for which the shape of the charging and discharging curves is almost linear [1–13]. Electrochemical capacitors can be classified as film-type (dielectric), electrolytic, and supercapacitors.

Electrolytic capacitors based on aluminum foils and liquid electrolytes are well known for many decades. In them, a thin film (thickness in the order of micrometers) of aluminum oxide prepared by electrochemically oxidizing the Al foils serves as a dielectric film. Their specific energy is of the order of some hundredths watt-hour per liter.

Electrochemical supercapacitors (ESCs) can be subdivided into electrical double-layer capacitors (EDLCs), pseudocapacitors, and hybrid-type capacitors. Historically, the first developed ESCs were EDLCs. Up to now they remain the most important ESC version. The first prototypes of electrical double layer (EDLs) were developed in the 1970s in Russia by N. Lidorenko and A. Ivanov [14] and also in Japan under the names "molecular energy accumulators" and "Ionistors."

The double-layer capacitor (EDLC) comprises two porous polarizable electrodes. The accumulation of energy in them proceeds through dividing positive and negative electrical charges between the two electrodes while maintaining a potential difference U between them. The electrical charge on each electrode depends on the EDL capacity. Due to a very low thickness of this layer (tenths of a nanometer), the capacity value referred to a unit of electrode's surface area is much higher than for electrolytic capacitors. Hence, the term "supercapacitor" was introduced.

In order to achieve high capacity values in EDLCs, highly dispersed carbonaceous electrodes with a high specific surface area of 1,000–300 m^2/g are used. An activated carbon (AC) or activated carbon cloths (ACC), alcogels, nanofibers, and nanotubes graphene sheets are used. Thus, the specific energy density of such capacitors reaches values of 1–20 Wh/L.

Y. M. Volfkovich · D. A. Bograchev (✉) · A. A. Mikhalin · V. S. Bagotsky
A. N. Frumkin Institute of Physical Chemistry and Electrochemistry, Russian Academy of Sciences, Moscow, Russia
e-mail: bograchev@gmail.com

Published online: 19 October 2013

For an EDLSC with ideal polarizable electrodes, the energy A delivered through a single discharge can be represented as:

$$A = (1/2)C\left[(U_{max})^2-(U_{min})^2\right], \quad (1)$$

where C is an average electrode's capacity, and U_{max} and U_{min} are the initial and the final values of discharge voltage, respectively. For full discharge until $U_{min}=0$, the maximal discharge energy will be: $A=A_{max}=(1/2)C[(U_{max})^2]$.

The development of EDLCs was induced by a necessity for rechargeable power sources with higher energy values, and power capabilities, and much better cyclability properties than those for existing storage batteries. Among the most remarkable features of EDLCs are excellent cyclability (hundred of thousands charge–discharge cycles as compared with hundreds or thousands of cycles for storage batteries) and the possibility to deliver for short periods high power and current densities, and also the possibility to be used at high and low temperatures (up to +60 °C and down to −50 °C). The cycling efficiency (ratio of energy consumed during charge and delivered during discharge) is about 92–95 %. Taking into account these properties, the following fields of applications for EDLCs in ICE vehicles (in parallel with storage batteries) are very promising for starting purposes with initial peak power (especially at low temperatures) and thus the increase of the battery life time and also in all-electric and in hybrid vehicles for energy recuperation during slow down and braking.

In *pseudocapacitors* electrical charges are accumulated mainly as the result of fairly reversible redox reactions (faradaic pseudocapacity). In many such reactions, oxides and sulfides of transition metals RuO_2, IrO_2, MnO_2, TiO_2, TiS_2, or their combinations take part [44–53].

One of the important achievements of modern electrochemistry is the development of *electron-conducting polymers* [1, 2, 54–65]. Electrochemical reactions in systems with conjugated double bonds such as polyaniline, polythiophene, polypyrrole, and others are reversible and can be used in supercapacitors. Such processes are called electrochemical doping or dedoping of the polymers with anions and cations. The electron conductivity during doping is due to the formation of delocalized electrons or electron holes and their migration in the system of polyconjugated double bonds under the influence of an applied electrical field. The use of some electron-conducting polymers as supercapacitor electrodes is based on the high reversibility of doping and dedoping reactions and the high conductance values of such polymers. The specific energy values of pseudocapacitors are fairly high 10–50 Wh/L and their cyclability reaches hundred thousands cycles. A disadvantage of supercapacitors based on transition of metal oxides and sulfides is their high price. A disadvantage of those based on electron-conducting polymers is their insufficient stability.

Some nonaqueous electrolytes supercapacitors with very high power and energy densities have been developed [66–70].

Recently, some *hybrid-type supercapacitors* have been developed in which different types of electrodes are used. In [15–18, 44, 71], capacitors were investigated in which the positive electrodes were based on metal oxides, and the negative electrodes were based on activated carbon, e.g., the system NiOOH/KOH/AC or the system PbO_2/H_2SO_4/AC. In both systems, conventional electrodes from alkaline or lead acid storage batteries were used. An advantage of the hybrid-type supercapacitors as compared with their analogues, with symmetrical AC, is their higher U_{max} value and correspondingly their higher specific energy (up to 10–20 Wh/kg). Symmetric AC systems have lower U_{max} value because an oxidative carbon corrosion is observed at not very high anodic potentials (0.9–1.0 V), while hydrogen evolution potential on the hybrid's negative AC electrode remains at high negative values up to −0.8 V. An advantage of hybrid supercapacitors over the corresponding storage batteries is much higher cycling capability, and the possibilities of faster charging and of easier hermetically sealing. Hybrid PbO_2/H_2SO_4/AC capacitors are used in wheelchairs and in electrical motor buses.

In [19], a hybrid supercapacitor with a RuO_2 positive electrode and an AC negative electrode was described. A high specific energy of 26.7 Wh/kg was reported.

An important feature of supercapacitors in comparison with storage batteries is possibility of rapid charge and discharge in very broad time intervals ranging from less than 1 s to several hours. Correspondingly, supercapacitors can be subdivided into power units with high values of specific power and into energy units with high specific energy values.

Power supercapacitors allow carrying out the charge and discharge processes in very short time periods (from fractions of a second to minutes) and obtaining herewith high power characteristics from 1 to 5 kW/kg in concentrated aqueous solutions with high specific conductivity. Measurements for highly dispersed carbon electrodes in the energy capacitor operation modes usually give the specific charge values in the range of 40 to 200 C/g [20, 21]. In the case of carbon materials, the limiting capacity obtained in [22] was 320 F/g due to a considerable contribution of pseudocapacitance of reversible surface group redox reactions. Thus, they are not pure DLC anymore. In [23], high power characteristics (above 20 kW/kg) were obtained for electrodes based on single-wall carbon nanotubes (SWCNT). Such high power values can be explained by regularity of the SWCNT's pore structure.

Energy-type ECSCs often use electrodes on which rather reversible faradaic processes occur. Such electrodes can be based on electron–conducting polymers (polyaniline, polythiophene, polypyrrole, etc) and also on some oxides of variable–valence metals (oxides of ruthenium, iridium, tungsten, molybdenum, zirconium, etc.) [1, 2]. They have different limitations for

practical application, such as expensiveness, insufficient durability due to degradation processes, etc. Using nonaqueous electrolytes in ECSC with electrodes based on highly dispersed carbon materials allows obtaining high (up to 3–3.5 V) charge voltage values, which significantly enhances the energy but limits the power of capacitors due to low conductivity of these electrolytes [1, 2, 24]. Aqueous alkali solutions allow obtaining rather high power values, but the low operating voltage range (about 0.8 V) decreases energy characteristics of ECSC. Aqueous electrolytes with the highest conductivity are sulfuric acid solutions with concentrations from 30 to 40 %. Besides, the working voltage range in the region of reversible processes proves to be above 1 V due to relatively low corrosion activity towards carbon as compared to other aqueous electrolytes.

In [25], high specific amount of electricity of 1,150 C/g was obtained for the first time for electrodes based on ADG-type activated carbon with the specific surface area of 1,500 m^2/g. This value was reached in the AC deep cathodic charge process to the potentials of –0.3 to –0.8 V RHE. It was assumed on the basis of these data and also on the basis of other various experiments that such a high amount of electricity is obtained as a result of hydrogen intercalation into AC carbon limited by solid-phase diffusion. These experiment data are as follows: a very slow (20 h and more) deep charging process, memory effect under potential scanning in the positive direction, absence of correlation between the specific surface area and specific capacitance values, linear dependence of current maximums on the square root of the potential sweep rate, and some other experimental data. It was concluded in this paper that the most probable limiting amount of electricity corresponds to the formula of C_6H which is similar to the formula of C_6Li for negative carbon electrodes of rechargeable lithium-ion cells. Nevertheless, it will be noted as a criticism that formation of the C_6H compound according to Faraday's law requires consumption of 1,320 C/g that was not reached in [25]. Herewith, the overall specific charge must be much higher than this value due to the presence of the EDL capacitance and pseudocapacitance of redox reactions of surface groups.

Therefore, the aim of the present work was to reach the maximum possible capacitance values on AC and also a more detailed study of mechanisms of the processes occurring under deep cathodic charging. Besides, the aim of the work was to develop a mathematical model of these processes and to compare it with experimental data.

There are only few papers on mathematic modeling of processes in ECSC. In [26], a DLC model was developed taking into account EDL charging, potential distribution in a porous electrode due to ohmic energy losses, and its porous structure. The calculation results were compared with the galvanostatic charging–discharge AC-based DLC curves that agreed well with each other. In [27, 28], the theory of operation was developed for electrodes based on electron-conducting polymers used in supercapacitors. The theory takes into account EDL charging, potential distribution in a porous electrode, electrochemical kinetics, intercalation of counterions in the polymer phase, and a nonsteady-state solid-phase diffusion of counterions in this phase. Simulation of the experimental discharge curves allowed obtaining the values of the parameters of processes occurring in the electrode: the solid-phase diffusion coefficient, EDL specific capacitance, and exchange current density of the electrochemical reaction. In [29], a model of a SWCNT electrode was developed taking into account EDL charging, hydrogen electrosorption–desorption, and kinetics of hydrogen electrooxidation–electroreduction according to the Volmer theory. In [30], the AC-based electrode impedance model accounted for EDL charging and intercalation nature of pseudocapacitance using statistical thermodynamics. However, there was no comparison between the theory and experiment in [29, 30].

Experimental methods

The following electrochemical methods were used in this work: the cyclic voltammetry, galvanostatic, and impedance techniques. The electrochemical impedance spectra were obtained using an electrochemical measurement system consisting of a Solartron 1255 frequency analyzer, Solartron 1286 potentiostat, and a computer, and also using a FRA impedance meter. Measurement of CVs and galvanostatic curves was carried out using Solartron 1286 and PI-50 potentiostats. Prolonged cell cycling was achieved using a Zaryad 8k cycling device. Apart from the impedance technique, the dc charged electrode resistance was measured as follows. After deep anodic charging, the cell was disassembled and the working electrode was removed. Further, in order to remove the acid residue, the electrode was dried in contact with microporous acid proof filter paper. Then, it was placed into a special four-electrode measurement cell and pressed between two liners of foil of thermally expanded graphite; copper disks with copper current leads were placed on the rear sides of this set. Further, the cell was sealed and the dependence of voltage on current was measured, from which the electrode resistance was calculated. An important feature of the method is that the cell with copper current leads must be assembled in a predetermined period of time (in our case, 3 min), as a deeply charged electrode undergoes gradual oxidation in air. An advantage of this method over impedance analysis is that it allows eliminating the polarization contribution into resistance as in the case of the impedance technique. Due to the above limitations, we used both of these methods.

Principal electrochemical studies were carried out in a specially designed Fluoroplast filter press cell with carbon current leads that allowed performing studies in a wide range of potentials. Its scheme is shown in Fig. 1 and its photograph is presented in Fig. 2. Figure 3 shows schematically the

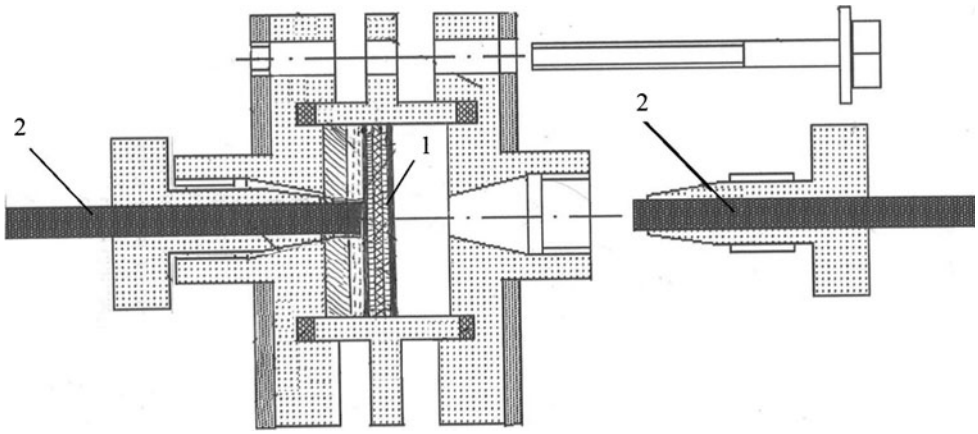

Fig. 1 Electrochemical cell. The principal details: *1*—electrochemical group, *2*—graphite current leads

electrochemical group of this cell representing a matrix system, in which the electrolyte is in the pores of the electrode and separator. The separator is clamped between two ring-shaped acid proof rubber gaskets that are chosen depending on the electrode thickness to provide reliable separation of the working and auxiliary electrodes. A fine texture Grace-type separator (polyethylene with silica gel) was used in the cell. Capacitance of the AC auxiliary electrode was much higher than that of the working electrode, which allowed eliminating interaction of electrodes through the evolved gas. Application of graphite current leads instead of the usual metallic (most often, platinum) ones allowed reaching high negative potentials (up to –1 V RHE), which in its turn provided obtaining ultrahigh capacitance values (see below).

The electrolyte used in this paper was mainly concentrated sulfuric acid with the concentrations from 30 to 60 %. The electrode used was the CH900-20 ACC (Japan). The electrodes had the surface area of 3 cm^2 with the thickness (in the compact state under the pressure of 0.5 MPa) of about 0.4 mm and the mass of about 0.06 g.

Studies of the porous structure and hydrophilic–hydrophobic AC properties were carried out using the method of standard contact porosimetry (MSCP) technique [31, 32] with evaporation of octane and water. The method is based on the laws of capillary equilibrium. If two (or more) porous bodies partially filled with a wetting liquid are in capillary equilibrium, the values of the liquid's capillary pressure $p^c=2\sigma\cos\theta/r$ (Laplace equation) in these bodies are equal, where r—pore radius, σ—surface tension, and θ—wetting angle. In this method, the amount of wetting liquid in the test sample (V_t) is measured. Simultaneously, the amount of the same wetting liquid is measured in a standard specimen of known porous structure (V_s). The liquids in both porous samples are kept in contact. After some time, a thermodynamic equilibrium is reached. The measurements are performed for different overall amounts of the liquid $V_0=V_s+V_t$. During the experiment, this overall amount is changed by gradual evaporation of the liquid. The MSCP with appropriate standard samples can be used to measure pore sizes in the range from 1 to $3\cdot10^6$ nm.

The MSCP has several substantial advantages over mercury porosimetry and other porosimetric methods. It has the possibility for the following:

- To investigate materials with low mechanical strength (for example clothes), frail materials, and even powders;
- To measure samples at fixed levels of compression and/or temperature, i.e., under conditions in which they are commonly used in different devices;

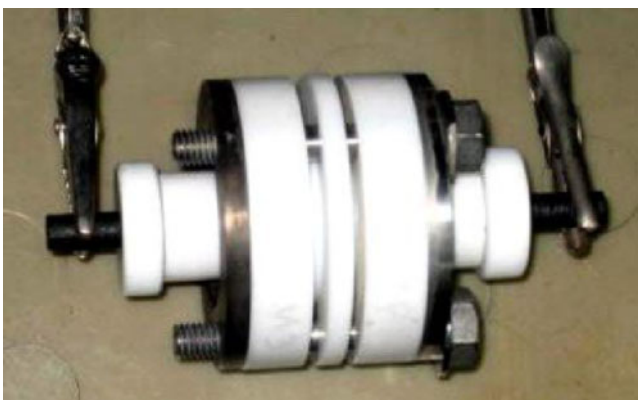

Fig. 2 Photograph of the electrochemical cell

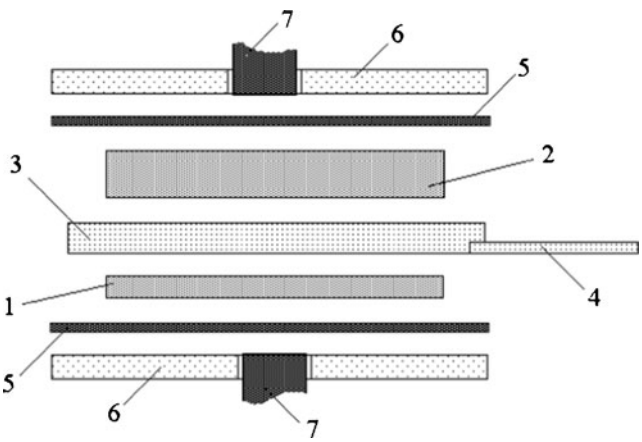

Fig. 3 Electrochemical group of the Fluoroplast cell. The principal details: *1*—test electrode, *2*—counter electrode, *3*—porous electrode, *4*—film of reference electrode, *5*, *7*—graphite currents collectors, *6*—frame

– To use for measurements the same liquid (for example water or water solutions) as that used in real devices (i.e., leading to the same swelling degree of the sample);
– Absence of the use toxic material such as mercury.

One of the most pronounced advantages of the MSCP is the possibility to investigate the wetting (hydrophilic/hydrophobic or lyophilic/lyophobic) properties of porous materials. Primarily, the MSCP measures the distribution of pore volume versus the capillary pressure p^c, i.e., versus the parameter $r^*=r/\cos\theta$ (henceforth, this parameter is called effective pore radius). For partially hydrophobic materials (for which $\theta>0$), the porosimetric curves measured with water are shifted towards higher values of r^* with respect to the curves measured with octane that wets most materials almost ideally ($\theta=0°$). The value of this shift for a certain value of pore volume V_n and of the corresponding pore radius r_n allows determining the wetting angle of water for pores with the radius r_n:

$$\cos\theta = r_n/r^*. \quad (2)$$

In porous materials, the wetting angles $\theta(r)$ for pores of different size can be different.

Experimental results and discussion

Figure 4 presents integral pore radius distribution curves measured using MSCP with octane and water for the CH900-20 AC cloth. As follows from this figure, this cloth has a very wide pore spectrum: from micropores with radii $r\leq1$ nm to macropores with $r>100$ nm, i.e., there are more than 5 orders of magnitude in the range. It is of interest that this cloth contains micropores and also macropores with $r>1$ μ, but there are practically no mesopores with 1 nm$<r<$50 nm. Micropores provide high full specific surface with s_f=1,520 m^2/g and hydrophilic specific surface s_{phi}=850 m^2/g. According to [32], porometric curves are measured using octane for all pores and using water only for hydrophilic pores. As follows from these curves, full porosity (by octane) was 86 %, hydrophilic porosity was 78.5 %, and hydrophobic porosity is 7.5 %.

Figure 5 presents the dependence of wetting angle θ on the pore radius calculated from Fig. 5 according to [32]. As may be seen, the θ values for the whole pore radius range are close to 90°. Therefore, though most of the pores are hydrophilic with $\theta<90°$, they are still badly wetted. The complex curve character in Fig. 5 is largely due to a nonuniform distribution of surface groups in the pores of different radii.

X-ray diffraction measurements of samples CH900-20 have been provided [33] for analyzing of interatomic structure. The obtained spectrum is presented in Fig. 6, as it may be noted this carbon has amorphous structure and a crystal phase does not take place. The domination of amorphous phase can slow down the rate of diffusion and respectively intercalations in the electrodes.

In this work, studies of AC were carried out in the large range of potentials from –0.8 to 1.0 V RHE. It is convenient to present the CV data obtained for more graphic representation of capacitance properties, especially those measured at different potential sweep rates (w), in the form of capacitance–voltage curves constructed in the coordinates of differential capacitance (C)–potential (E), where $C=dQ/dt=I\,dt/dE=I/w$, I is the current, Q is the charge accumulated, $w=dE/dt$, and t is the time.

Figure 7 compares the cyclic capacitance–voltage curves measured in 48.5 % H_2SO_4 at different potential sweep rates in two ranges of potentials: in the reversibility range (from 0.1 to 0.9 V) and in the deep charging range (from –0.8 to 1 V). As follows from curve 4 measured in the reversibility range, only EDL charging occurs here, while pseudocapacitance of redox reactions of surface groups is very low in this case. This distinguishes the CH900-20 ACC from ADG AC in which considerable contribution is introduced by pseudocapacitance of fast redox reactions of surface groups [25]. As follows from curve 4, the value of EDL capacitance is approximately 160 F/g. Taking into account that s_{phi}=850 m^2/g, we obtain C_{DEL}=18.8 μF/cm^2 of the true hydrophilic carbon surface. This value is close to the

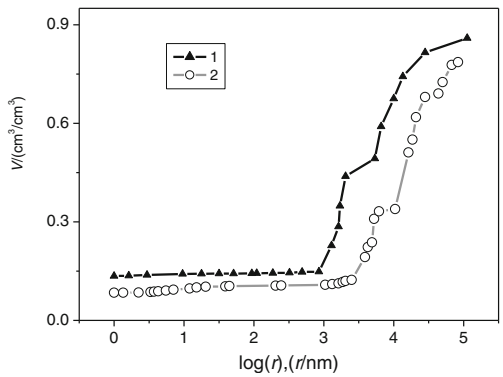

Fig. 4 Integral pore radius distribution curves measured in octane (*1*) and water (*2*) for a CH900-20 AC cloth

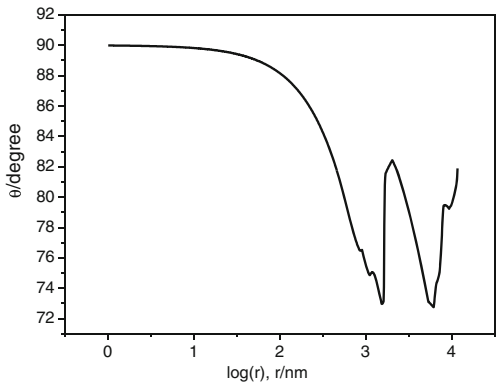

Fig. 5 Dependence of wetting angle θ on the pore radius for the CH900-20 AC cloth

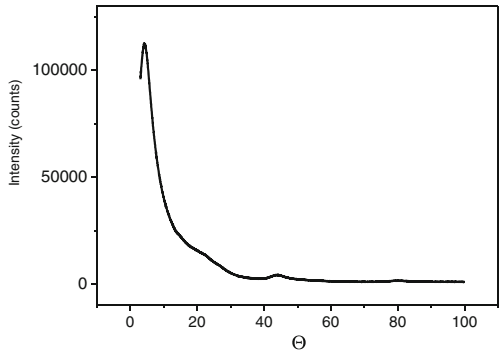

Fig. 6 XRD pattern of CH900-20

classical EDL capacitance value of platinum [34]. Much lower C_{EDL} values presented in [35], in our opinion, are explained by the fact that the values of full specific surface area measured using the BET technique are used, while it is known that carbon materials have both hydrophilic and hydrophobic pores. While RCP used in this work allows obtaining the s_{fi} values and thus the C_{DEL} values per only working surface area, i.e., hydrophilic surface area.

In the range of negative potentials (←–0.1 V) (curves 1, 2, 3), faradaic processes with a very high pseudocapacitance are observed. As may be seen, the EDL capacitance decreases in the range of negative potentials. This is probably due to the partial surface blocking by adsorbed particles. There are two pronounced maxima in the anodic branches of curves 2 and 3 measured at low w values, which points to the probable occurrence of two slow processes. There is a single deep maximum corresponding to a very high amount of electricity under deep cathodic charging of AC in cathodic branches of curves 1, 2, and 3.

The method of galvanostatic curves was used to measure the amounts of electricity after long-term charging at negative potentials. Figure 8 presents the dependence of specific amount of charge Q under discharge on the charge time at potential E =–250 mV in 40.3 % H_2SO_4. As may be seen, the Q value grows very fast at very low charging times of seconds and minutes and continues increasing further for many tens of

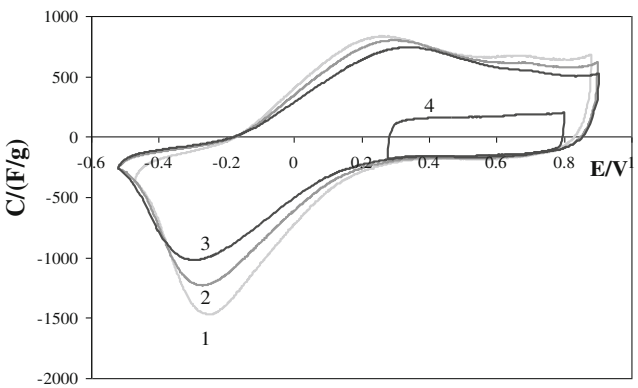

Fig. 7 Capacitance–voltage cyclic curves for CH900-20 for 48 % H_2SO_4 at potential rates: *1*—0.5 mV/s, *2*—1 mV/s, and *3*, *4*—2 mV/s

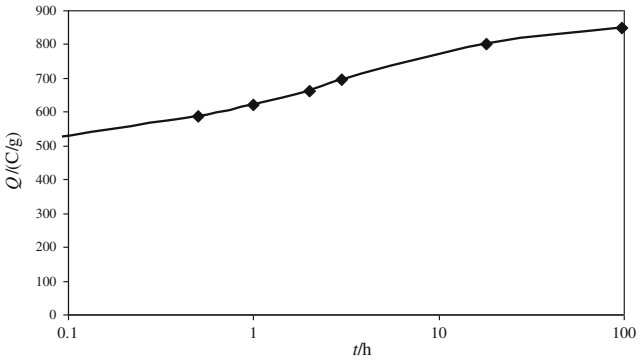

Fig. 8 Dependence of specific amount of charge under discharge of the CH900-20 electrode in 40.3 % sulfuric acid on the charging time under the charging potential of 250 mV

hours. Such very slow growth can be explained by very slow diffusion. It is known that the lowest diffusion coefficients are observed in the solid phase; they are lower by orders of magnitude than in the liquid phase. In this connection, one may assume occurrence of hydrogen intercalation into AC carbon controlled by slow solid-phase hydrogen diffusion. This is also evidenced by proportionality of the limiting current to a square root of the potential sweep rate and also by a number of other experimental data obtained in [25] (memory effect under potential sweep in the positive direction, absence of correlation between the specific surface area value and specific capacitance, etc.) It is assumed in the same work [25] that compound C_xH and the limiting C_6H compound is formed in the course of hydrogen intercalation under AC deep cathodic charging. As already shown above, one may assume on the basis of the shape of potentiodynamic curves that two slow processes may occur, of which the slower process is solid-phase diffusion intercalation of hydrogen into AC carbon and the faster process is probably hydrogen chemosorption at the interface of carbon and electrolyte in pores.

Figure 9 presents the dependence of active high-frequency series resistance at 1 kHz of the electrode on the charging time at E =–400 mV measured using the impedance technique in 40 % sulfuric acid. As may be seen, active resistance of the electrode grows in the course of the charging process. However, both the solid phase and electrolyte in pores contribute to the resistance. The dependence of electric resistance on the charging time measured under constant current according to the above technique is more significant.

Figure 10 presents such a dependence of the dc electron resistance of a CH900-20 electrode on the charging time in 40.3 % sulfuric acid at E =–0.34 V. As seen from this figure, the electrode resistance grows significantly at an increase in the AC charging time. One should keep in mind that the above parameters were obtained on activated carbon cloth (CH900-20), which practically eliminates the effect of contact resistance between its separate fibers, as one may assume the fibers to represent practically parallel transport paths for electrons.

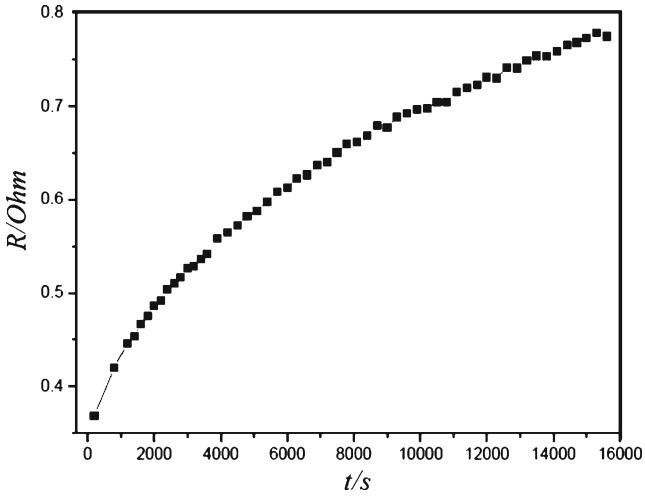

Fig. 9 Dependence of active resistance of the electrode on the charging time at E =–400 mV measured using the impedance technique in 40 % sulfuric acid

Therefore, the above data may be explained by a change in the bulk phase chemical composition in the course of charging. Thus, both resistance measurement techniques point to its increase as dependent on the charging time. This can also be explained by a change in the solid phase composition: from C to C_xH and, in the limit, to C_6H.

The maximum specific charge of 1,560 C/g was obtained from galvanostatic discharge curves after potentiostatic charging for 22 h at the potential of E =–0.31 V RHE in 56.4 % H_2SO_4. In this case, the integral specific capacity is equal to 1, 560 C/g/1.4 V ~ 1,110 F/g. Authors do not know the close values which have been obtained on the base of AC electrodes by other researchers.

Figure 11 presents the dependence of the maximum specific charge of CH900-20 on the sulfuric acid concentration (in the range from 34 to 56 %) for the discharge time of 18 h for each concentration.

As follows from Fig. 11, the specific charge grows at an increase in the sulfuric acid concentration. On the other hand,

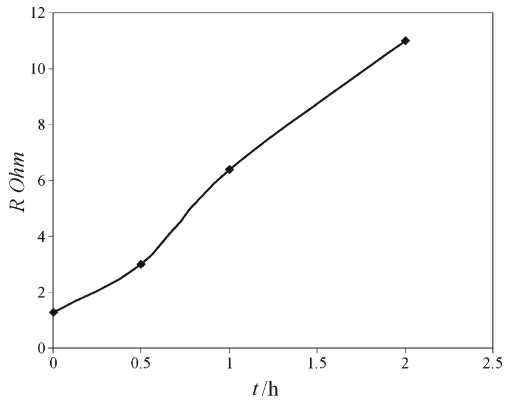

Fig. 10 Dependence of electron resistance of the CH900-20 electrode on the charging time in 40.3 % sulfuric acid at E =–0.34 V measured under constant current

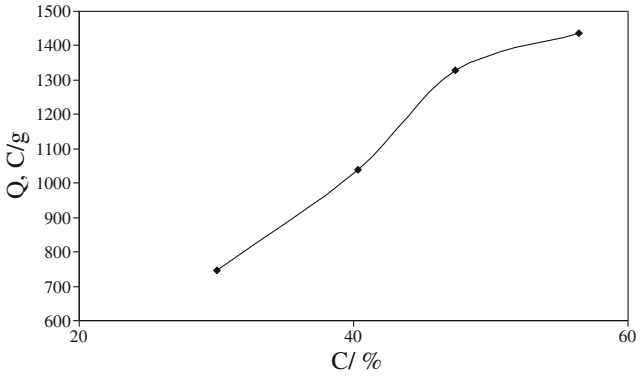

Fig. 11 Dependence of the maximum specific charge of CH900-20 on the sulfuric acid concentration for the charging time of 18 h

the following facts are known from the literature: (1) Acid intercalation into graphite and graphite-like materials occurs in concentrated sulfuric acid solutions that are enhanced at an increase in the concentration [36–38]. Herewith, the gap between carbon microstructures where the acid penetrates grows. Their swelling to a certain degree occurs under adsorption of different adsorptives on activated carbons [39]. As graphite-like impurities are contained in AC [40, 41], then one may assume on the basis of all these data that *double intercalation* occurs in our case. Sulfuric acid is intercalated into AC expanding the gaps space. Hydrogen atoms are then directed into this space under deep cathodic charging of AC. This space serves as a transport route for hydrogen. Then, it interacts with carbon with the ultimate formation of compound C_6H (*carbon hydride or hydrogen carbide*) (see Fig. 12).

According to Faraday's law, formation of compound C_6H requires 1,320 C/g. (F/M_{C6H} 96,500 C g-equiv^{-1}/73 g-equiv g^{-1}) The maximum value of Q_{max}=1,560 C/g was obtained in our paper. Therefore, other rechargeable processes require 240 C/g. This value includes in the first instance the value of $Q_{EDL}=C_{EDL}\times\Delta E$, where ΔE is the range of potentials. In this case, ΔE=1.4 V, so to the first approximation, C_{EDL}=240/1.4=170 F/g. This is approximately the same value as the one obtained from curve 4 in Fig. 7. However, this is an approximate estimate, as the C_{EDL} value somewhat depends on the potential and also as a small contribution into the Q_{max} value is made by pseudocapacitance of redox

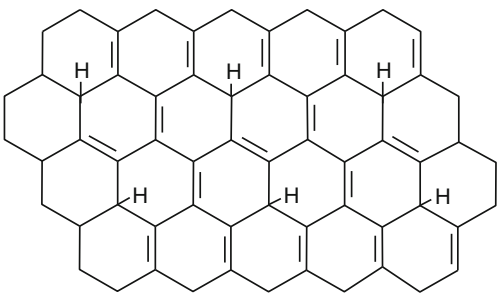

Fig. 12 Structural formula of compound C_6H

reactions of surface groups. Nevertheless, this approximate estimate shows the correctness of the assumed mechanism of deep AC charging. Herewith, one must take into account that though the Q_{max} value is eventually determined by the slowest process of hydrogen intercalation controlled by its solid-phase diffusion, but as already assumed above, hydrogen chemosorption occurs on the interface of carbon/electrolyte in pores at earlier electrode charging stages. Though the process of electrochemical chemosorption on the interface and the bulk process of hydrogen intercalation occur at different rates, both of them eventually lead to formation of the single bulk compound C_6H.

Figure 13 presents the obtained dependence of Q on the charging potential for C_{H2SO4}=40.3 %. For Fig. 13 at C_{H2SO4}=40.3 % during the first 18 h potentiostatic charge carried to different potentials and then galvanostatic discharge was used at a current density of 1.2 mA/cm^2, one may see that the curve reaches a plateau at $E \leftarrow 250$ mV. The very fact of reaching a plateau points to a saturation of carbon bulk (and surface) by hydrogen atoms, i.e., evidences indirectly the thermodynamic saturation of the C_x–H chemical bonds at the given potential and H_2SO_4 concentration.

Thus, neither the further increase in the concentration of H_2SO_4 above 56.4 % nor the further decrease in the charging potential below –250 mV nor any increase in the charging time results in an increase in the maximum specific charge Q_{max} 1,560 C/g. As pointed out above, the contribution into this DEL capacitance value is 240 C/g, so the dominating contribution to the Q_{max} value is made by specific charge Q=1,320 C/g corresponding to formation of the C_6H compound (pseudocapacitance charge). In principle, if one uses other activated carbons and cloths, the DEL capacitance value may somewhat increase due to an increase in the AC specific surface area that in our case is S_f=1,520 m^2/g. However, this must not affect any significant growth of the Q_{max} value.

Galvanostatic cycling of the CH900-20 electrode was carried out at the current density of 1.2 mA/cm^2 in the range of potentials from –0.32 to 1.03 V. Figure 14 presents the dependence of specific discharge capacitance Q on number of cycles N for C_{H2SO4}=48.5 %. C_{H2SO4}=48.5 % galvanostatic cycling was carried out at a current density of 1.2 mA/cm^2 in the potential range from −0.3 to 1 V.

One may see that the Q value changed little in 100 cycles. Then, the cycling was stopped, as it had already taken a lot of time: 588 h. The mean Q value was 940 C/g. At N=100, the obtained overall discharge capacitance is 26.3 A h/g. Figure 15 presents cyclic charge–discharge curves for 8 cycles. The difference between these curves and the ideal "sawtooth" is related to occurrence of the above pseudocapacitance processes. As its specific charge has not changed significantly after a long cycling of the electrode, it can be concluded that the electrode material has not been degraded

Besides the studies of deep cathodic charging of CH900-20 ACC in H_2SO_4 solutions, a similar measurement was carried out for 90 % aqueous H_3PO_4 solution. The specific charge value calculated using this plot is 1,200 C/g. As according to [38], phosphoric acid is intercalated into graphite and graphite-like compounds, these results agree with the above mechanism of double intercalation of H_3PO_4 and hydrogen into AC during deep cathodic charging.

The above data point to high prospects of using ACs under the conditions of deep cathodic charging for high energy density supercapacitors.

Mathematic charge–discharge model of electrode based on activated carbon

Macrokinetics models of ions intercalation in the porous electrodes are widely reported in literature, especially in relation to the lithium-ion systems. The models taking into account the diffusion of the electrolyte and solid phases originate from works [72] on the modeling of lithium-ion battery with two electrodes. There is an easier approach which focuses on only cathode properties and neglects processes of diffusion in all phases, see for instance [73].

Single-electrode systems with intercalation were considered in works [74, 75]. Work [74] took into account the influence of the presence of electrode particles of different

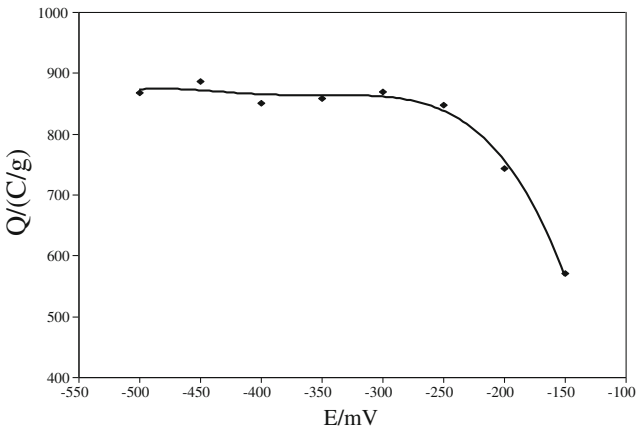

Fig. 13 Dependence of specific capacitance on the potential of charging for 18 h in 40.3 % H_2SO_4

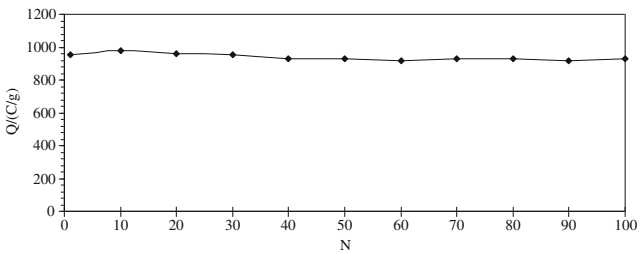

Fig. 14 Dependence of specific discharge capacitance Q on the number of cycles

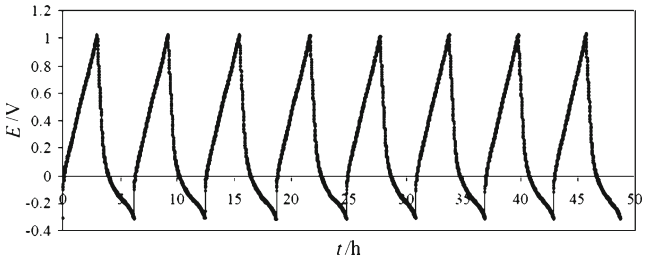

Fig. 15 Cyclic charging–discharge curves for 8 cycles

sizes. The nonlinear diffusion of intercalated ions in solid phase was studied in work [75]. Considerations of intercalation kinetics based on Frumkin isotherm were reviewed in paper [76].

Figure 16 shows the scheme of microstructure of AC electrode based on the results of the above structural measurements (see Figs. 4, 5, and 6). The scheme supports the mathematical model developed in the paper. The scheme reflects the presence of either hydrophilic pores filled electrolyte solution or hydrophobic gas-filled pores. Atomic hydrogen generated at the interface of the electrolyte/carbon during process of intercalation in the carbon diffuses into the solid phase inside the hydrophilic pore walls of the normal to its surface.

We developed a quasi two-dimensional mathematical model of charge–discharge for highly dispersed carbon taking into account the obtained experimental results.

Hydrogen solid-phase diffusion is assumed to be one dimensional. Then, the equation for hydrogen diffusion may be written in a one-dimensional form:

$$\frac{\partial c}{\partial t} = D\frac{\partial^2 c}{\partial x^2}, \tag{3}$$

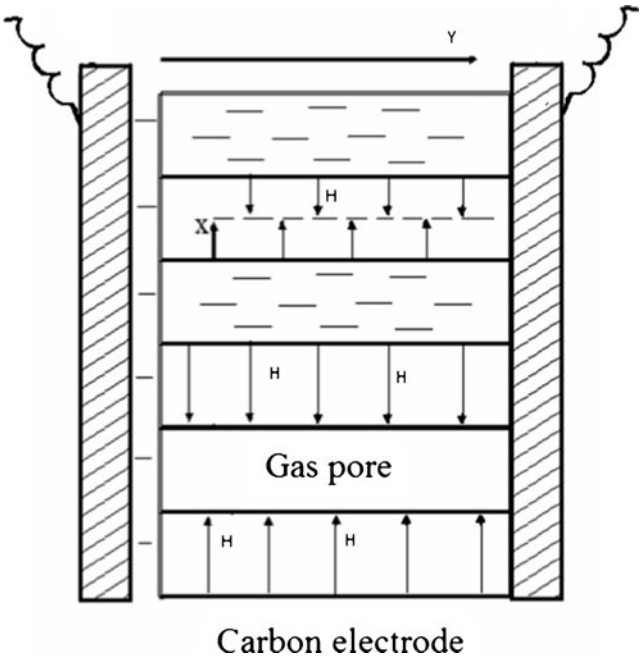

Fig. 16 Scheme of microstructure of AC electrode

where c is the hydrogen concentration in the AC, t is the time, x is the shortest axial coordinate, and D is the solid-phase diffusion coefficient of hydrogen. The boundary condition at the interface of carbon/electrolyte in pores is:

$$i_{\text{in}} = nFD\frac{\partial c}{\partial x}\bigg|_{x=0}, \tag{4}$$

where n is the charge transferred, F is Faraday's number, i_{in} is the current density determined by the kinetic dependence of the reaction. Let us also assume that there is a certain length H corresponding to half thickness of average pore wall, where there is no hydrogen diffusion flux due to the symmetry:

$$0 = \frac{\partial c}{\partial x}\bigg|_{x=H}. \tag{5}$$

The intercalation current density is determined by the Butler–Volmer kinetics:

$$i_{\text{in}} = i_0\left(1-\frac{c_s}{c_H}\right)^{1-\alpha}\left(\frac{c_s}{c_H}\right)^{\alpha}\left(e^{\frac{\alpha\left(U-E_{\text{ref}}(cs)\right)F}{RT}} - e^{-\frac{(1-\alpha)\left(U-E_{\text{ref}}(cs)\right)F}{RT}}\right), \tag{6}$$

where i_0 is the exchange current density, c_s is the hydrogen concentration at the interface, α is the charge transfer coefficient, and $E_{\text{ref}}(c_{\text{s}})$ is the reference potential as function of concentration.

Let us assume that the initial state of the discharge process is saturation of carbon by hydrogen; then, the initial condition for Eq. (2) is:

$$c = c_H|_{t=0}, \tag{7}$$

The EDL capacitance current may be written as [42]:

$$i_{\text{EDL}} = C_{\text{EDL}}\frac{\partial U}{\partial \tau}, \tag{8}$$

Intercalation and EDL charging currents are included into the equation determining the polarization distribution across the porous electrode thickness that may be presented as:

$$\frac{\partial}{\partial y}\left(\kappa\frac{\partial U}{\partial y}\right) = Si_{\text{EDL}} + Si_{\text{In}} \tag{9}$$

where κ is the conductivity of electrolyte in the pores determined according to the Archie relationship: $\kappa = \kappa_0\varepsilon^2$ [43], S is the specific surface area (with dimension—1/cm), and ε is the porosity. It was assumed in Eq. (9) that specific conductivity of the carbon material is much higher than that conductivity of electrolyte.

It is well known that electrical conductivity of carbon is 3–4 orders higher than electrical conductivity of electrolytes, thus even the conductivity several times reduced (see Fig. 9 and Fig. 10) by changes in composition of the electrode solid phase from C to C_xH during charge and discharge allows not taking

into account the electrical conductivity of the electrode in the model.

The H value may be provisionally determined on the basis of the literature on activated carbons [39]: $H \sim 1/(s_{\mathrm{phi}}\ \rho)$, where ρ is the measured effective density of carbon taking into account the gas pores $\rho \sim 1.2$ g/cm^3. It is assumed that specific surface of the hydrophilic pores is $s_{\mathrm{phi}}=0.85\times 10^7$ cm^2/g, $H \sim 1$ nm.

In the case of the galvanostatic mode, the boundary conditions for Eq. (9) are written as:

$$-\kappa\frac{\partial U}{\partial y}\bigg|_{y=0} = I, \kappa\frac{\partial U}{\partial y}\bigg|_{y=L} = 0, \tag{10}$$

where L is the porous electrode thickness. I is the overall current density per electrode unit visible surface. The condition (10) implies that on the left side of model ($y=0$) the total electrical currents flow through the electrolyte, and on the model right side (y = L) there is an insulation condition for electrical currents in the electrolyte.

System of Eqs. (3)–(9) with boundary conditions (10) is the system with parameters twice distributed along the x and y axes; it describes hydrogen intercalation and adsorption in the porous carbon structure and also EDL charging.

The important differences between the present model and the macrokinetic models developed in the literature are firstly, the neglect of concentration polarization in the electrolyte and, secondly, that diffusion in the solid phase is represented not with diffusion in spherical particles of the electrode but with diffusion in 1 dimensional volume. The first can be justified as electric currents in the system are not sufficiently high and the electrolyte concentration is important. The second can be supported by our ideas about the structure of the considered highly dispersed carbon with thin porous walls.

This system of equations was solved numerically using the FEM solver. The set of system parameters is presented in Table 1.

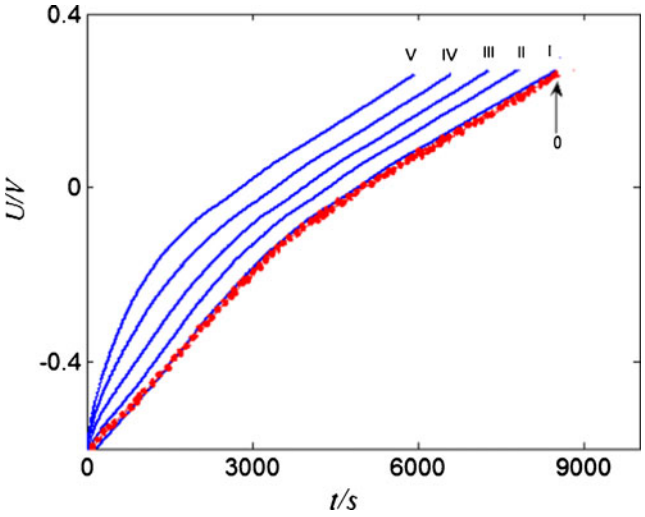

Fig. 17 The discharge curves for the current density 2 mA/cm^2, (*0*) the experimental curve, (*I*) the calculated curve with surface density value S taken from experiment, (*II*) the calculated curve with surface density value $S/2$, (*III*) the calculated curve with surface density value $S/3$, (*IV*) the calculated curve with surface density value $S/4$, (*V*) the calculated curve with surface density value $S/5$

Herewith, most of the parameters were taken from the experiment. The parameters obtained as a result of fitting of calculated and experimental galvanostatic discharge curves are D, i_0.

Figure 17 presents the results of simulation of the galvanostatic discharge curves (dependence of the potential on the discharge time) at the current density 2 mA/cm^2. This figure shows good agreement between the calculated and experimental curves (curve I and curve 0 correspondingly), which evidences the correctness of the model. The fitting yielded an approximate value of hydrogen solid-phase diffusion coefficient into AC carbon $D \sim 10^{-16}$ cm^2/s. As in Fig. 16, the calculated galvanostatic discharge curves for systems with smaller surface densities are shown.

Table 1 System parameters used for calculation

Parameter, [dimension]	Value	Source
The charge transfer coefficients α	0.5	Fitting
The hydrogen solid-phase diffusion coefficient D, [cm^2/s]	5×10^{-17}	Fitting
The half thickness of pore wall H, [cm]	10^{-7}	Fitting
The electrode thickness L, [cm]	0.05	Experiment
The exchange current density i_0, [A/cm^2]	0.5×10^{-8}	Fitting
The DEL specific capacitance C_{EDL}, [F/cm^2]	2×10^{-5}	Fitting
The specific hydrophilic surface S, [cm^{-1}]	2.03×10^{6}	Experiment
The porosity ε	0.86	Experiment
The limiting concentration of protons in carbon c_{H}, [mole/cm^3]	0.023	Fitting
The system temperature T, [K^0]	298	Experiment
The specific conductivity of electrolyte κ, [S/cm]	0.1	Experiment
The overall current density per unit visible surface I, [mA/cm^2]	2	Experiment

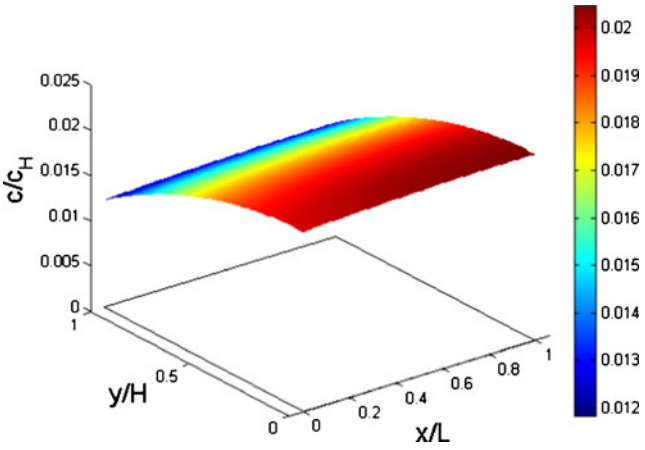

Fig. 18 Dimensionless concentration profile at the end of discharge with surface density *S*

The low coefficient of solid-state diffusion of hydrogen in carbon can be verified by semiquantitative analysis. Simple estimate shows that at very high specific surface area of carbon (1,500 m^2/g), pore wall thickness is about 1 nm. Obviously, if at the same time the deepest charge requires dozens of hours, it corresponds to very low coefficient of diffusion in the solid phase. .

The exchange current density $i_0=0.5\times10^{-8}$ A/cm^2 is not very different from the corresponding value for the lateral side of pyrographite $i_0=2.5\times10^{-8}$ A/cm^2 [77]. These values can be treated as close considering that these carbon materials have significantly different surface chemistry.

Figure 18 and Fig. 19 presents the distribution (profile) of dimensionless concentration at the end of discharge by two coordinates: *x* and *y*. One may see that almost uniform hydrogen concentration distribution, by both coordinates, *x* and *y*, occurs at the given system parameters (see Fig. 18) and strong nonuniform hydrogen concentration distributions take places in the case of smallest surface density (see Fig. 19).

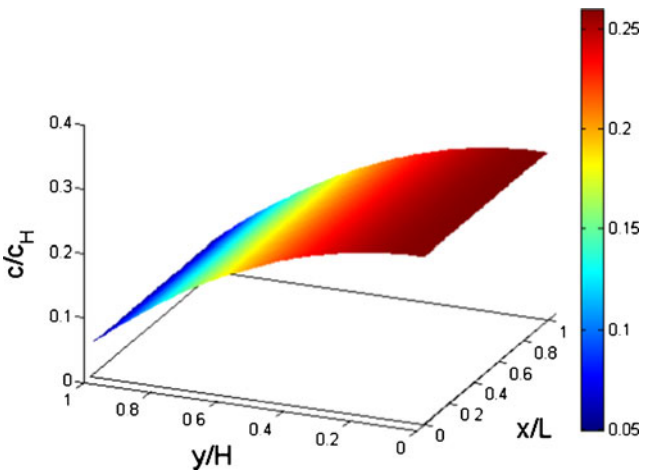

Fig. 19 Dimensionless concentration profile at the end of discharge with surface density *S*/5

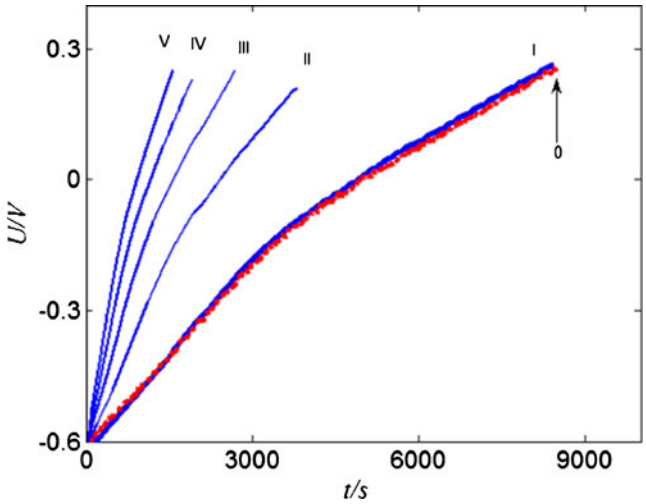

Fig. 20 The discharge curves for various current densities. (*0*) The experimental curve 2 mA/cm^2 and the calculated curves (*I*)—2 mA/cm^2, (*II*)—4 mA/cm^2, (*III*)—6 mA/cm^2, (*IV*)—8 mA/cm^2, (*V*)—10 mA/cm^2

The simulated galvanostatic discharge curves at different current densities have been demonstrated in Fig. 20. The capacitance decreases with increasing current density and correspondently increasing nonuniformity of hydrogen concentration distribution at the end of discharge (see Fig. 21 and compare with Fig. 18).

Conclusion

Electrochemical properties of electrodes based on CH900-20 AC cloth were studied in concentrated H_2SO_4 solutions in a wide range of potentials from –0.8 to +1 V RHE. Cyclic voltammetric curves measured in two ranges of potential were obtained in the reversibility range (from 0.1 to 0.9 V) and in the deep cathodic charging range (from –0.8 to +1 V). Electric double electric layer (EDL) charging occurs in the reversibility

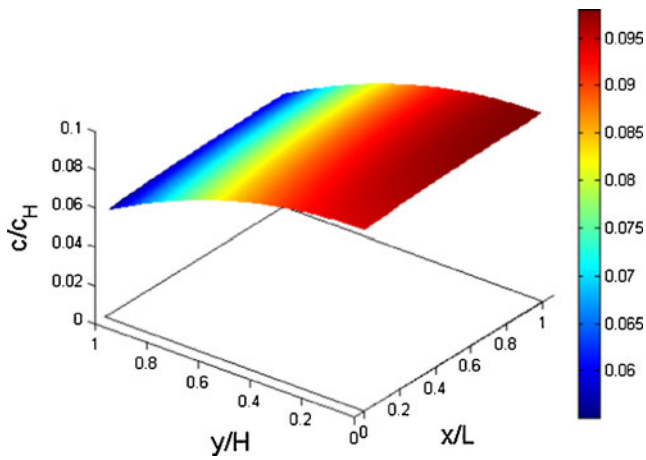

Fig. 21 Dimensionless concentration profile at the end of discharge with current density 10 mA/cm^2

range, while faradaic process of hydrogen intercalation into AC carbon takes place in the range of negative potentials (←−0.1 V). The intercalation process is controlled by slow solid-phase hydrogen diffusion into AC carbon. For the first time, the maximum value of specific discharge capacitance of 1,560 C/g (or 1,110 F/g) is obtained, which is much higher than values known from the literature for carbon electrodes. On the basis of this value and Faraday's law, it is concluded that the compound of C_6H is formed in the limiting case of AC deep cathodic charging. The specific charge value grows at an increase in the concentration of H_2SO_4 and also at an increase in the charging time.

The obtained experimental data allowed suggesting a mechanism of double intercalation under AC deep cathodic charging. Sulfuric acid is intercalated into AC expanding the interatomic space. Hydrogen atoms are then directed into this space. Eventually, it facilitates intercalation of hydrogen into carbon. Then, hydrogen atoms interact with carbon and the compound C_6H is generated in the limit. The obtained data were used to develop a model for an AC electrode taking into account the EDL charging and hydrogen intercalation.

Using of the observed electrodes system in energy type supercapacitors has good prospects according to the results of this work (very high discharge capacities can be achieved at deep cathodic charging of activated carbon-based electrodes to potential values from −0.1 to −0.5 V RHE). At the same time, the results allow explaining the high specific energy values (up to 20 Wh/kg) observed 10 years ago for hybrid (+)PbO_2/H_2SO_4/AY(−) supercapacitors [17, 18]. These high values were achieved at a maximal charging voltage U_{max} of 2.2 V. Taking into account that for the positive PbO_2 electrode E_{max}^{+}=1.85 V RHE and therefore the value of E_{min}^{-} was −0.35 V RHE corresponds to the region of maximal capacity for activated carbon-based electrodes.

References

1. Conway BE (1999) Electrochemical supercapacitors. Kluwer Academic/Plenum, New York
2. Volfkovich YM, Serdyuk TM (2002) Russ J Electrochem 38:935–959
3. Barsukov IV, Johnson C, Doninger E, Barsukov VZ (2006) New carbon based materials for electrochemical energy storage systems: batteries, supercapacitors and fuel cells. Mathematics, Physics and Chemistry. Springer, New York, NATO Science Series II
4. Kotz R, Carlen M (2000) Electrochimica Acta 45:2483–2498
5. Pandolfo AG, Hollenkamp AF (2006) J Power Sources 157:11–27
6. Simon P, Gogotsi Y (2008) Nature Materials 7:845–854
7. Chen Y, Zhang X, Yu P, Ma Y (2010) J Power Sources 195:3031–3035
8. Chen Y, Zhang X, Zhang D, Yu P, Ma Y (2011) Carbon 49:573–580
9. Lu W, Qu L, Henry K, Dai L (2009) J Power Sources 189:1270–1277
10. Stoller MD, Park S, Yanwu Z, An J, Ruoff RS (2008) Nano Letters 8: 3498–3502
11. Vivekchand RC, Rout CS, Subrahmanyam KS, Govindaraj A, Rao CNR (2008) J Chem Sci 120:9–13
12. Zhang H, Cao G, Yang Y, Gu Z (2008) J Electrochem Soc 155:K19–K22
13. Bakhmatyuk BP, Venhryn BY, Grygorchak II, Micov MM, Kulyk Y (2007) Electrochimica Acta 52:6604–6610
14. Lidorenko S (1974) Doklady Akademii Nauk USSR 216:1261–1267
15. Beliakov AI, Brintsev AM (1997) Proc 7th Int Seminar on Double Layer Capacitors and Similar Energy Storage Devices Deerfield Beach Florida 7
16. Beliakov AI (1998) Proc. 8th Int Seminar on Double Layer Capacitors and Similar Energy Storage Devices Deerfield Beach. Florida 8
17. Belyakov AI, Volfkovich YM, Shmatko PA (2001) US Patent 6 195 252 B1
18. Volfkovich YM, Shmatko PA (2003) US Patent 6 628 504
19. Zheng JP, Ding SP, Jow TR (1997) Proc 7th Int Seminar on Double Layer Capacitors and Similar Energy Storage Devices Deerfield Beach Florida
20. Fang B, Binder L (2006) J Power Sources 163:616–622
21. Centeno T, Stoeckli F (2006) Electrochimica Acta 52:560–566
22. Bleda-Martinez MJ, Agull JAI, Lozano-Caste D, Morall E, Cazorla-Amor D, Linares-Solano A (2005) Carbon 43:2677–2684
23. Volfkovich YM, Rychagov AY, Sosenkin VE, Krestinin AV (2008) Elektrokhimicheskaya Energetika 8:106–111
24. Izmailova MY, Rychagov AY, Den'shchikov KK, Volfkovich YM, Vygodskii YS, Lozinskaya EI (2009) Russ J Electrochem 45:949–950
25. Rychagov AY, Volfkovich YM (2009) Russ J Electrochem 45:304–310
26. Vol'fkovich YM, Mazin VM, Urisson NA (1998) Russ J Electrochem 34:740–746
27. Volfkovich YM, Bagotzky VS, Zolotova TK, Pisarevskaya EY (1996) Electrochimica Acta 41:1905–1912
28. Volfkovich YM, Sergeev AG, Zolotova TK, Afanasiev SD, Efimov ON, Krinichnaya EP (1999) Electrochimica Acta 44:1543–1558
29. Volfkovich YM, Petrii OA, Zaitsev AA, Kovrigina IV (1988) Vestnik MGU Ser 2 Khimiya 29:173-181
30. Fernandez S, Cartro EB, Real SG, Martines ME (2009) Internat J Hydrogen Energy 34:8115–8126
31. Volfkovich YM, Sosenkin VE, Bagotsky VS (2010) J Power Sources 195:5429–5441
32. Volfkovich YM, Bagotzky VS, Sosenkin VE, Blinov IA (2001) Colloid and Surfaces A: Physicochem Eng Aspects 187–188:349–365
33. Volfkovich YM, Mikhailin AA, Bograchev DA, Puryaiva TP, Shiryaev AA (2013) Supercapacitor electrodes with high pseudo-capacitance on the base of activated carbon poster presentation Book of poster, conference Actual problem of Adsorption, Porosity and adsorption selectivity. Moscow
34. Frumkin AN, Bagotskii VS, Iofa ZA, Kabanov BN (1952) Kinetika elektrodnykh protsessv (Kinetics of electrode processes). Moscow University Press, Moscow
35. Tarasevich MR (1984) Elektrokhimiya uglerodnykh materialov (Electrochemistry of carbon materials). Nauka, Moscow
36. Ubellode AR, L'yuis FA (1965) Grafit I ego kristallicheskie soedineniya (Graphite and its crystalline compounds). Mir, Moscow
37. Fialkov AS (1997) Uglerod, mezhsloevye soedineniya i kompozity na ego osnove (Carbon, interlayer compounds and composites on its basis). Aspect, Moscow
38. Sorokina NE, Nikol'skaya IV, Ionov SG, Avdeev VV (2005) Izv RAS Ser. Khim 54:1–9
39. Yakovlev VY, Fomkin AA, Tvardovski AV (2004) J Colloid Interface Sci 280:305–308
40. Rychagov AY, Urisson NA, Volfkovich YM (2001) Russ J Electrochem 37:1172–1179
41. Fenelonov VB (1995) Poristyi uglerod (Porous carbon). Izd. Instituta Kataliza SO RAN, Novosibirsk
42. Delahay P (1965) Double layer and electrode kinetics. Wiley, New York

43. Chizmadzhev YA, Markin VS, Tarasevich MR, Chirkov YG (1971) Makrokinetika protsessov v poristykh sredakh (Macrokinetics of Processes in Porous Media). Nauka, Moscow
44. Burke A (2000) J Power Sources 91:37–50
45. Kudo T, Ikeda Y, Watanabe T, Hibino M, Miyayama M, Abe H, Kajita K (2002) Solid St Ion 152–153:833–841
46. Xue Y, Chen Y, Zhang M, Yan Y (2008) Materials Let 62:3884–3886
47. Guang-lei C, Xin-hong Z, Lin-jiel Z, Thomas A, Müllen A (2007) New. Carbon Materials 22(4):302–306
48. Liang H, Chen F, Li R, Wang L, Deng Z (2004) Electrochimica Acta 49:3463–3467
49. Yue-feng S, Feng W, Li-ying B, Zhao-hui B (2007) New Carbon Mat 22(1):53–58
50. Li Z, Wanga J, Liua S, Liua X, Yanga S (2011) J Power Sources 196: 8160–8165
51. Crossa A, Morelb A, Cormiea A, Hollenkampc T, Donne S (2011) J Power Sources 196:7847–7853
52. Makino S, Yamauchi Y, Sugimoto W (2013) J Power Sources 227: 153–160
53. Kalubarme RS, Jadhav HS, Park C (2013) Electrochimica Acta 87: 457–465
54. Snook GA, Kao P, Best AS (2011) J Power Sources 196:1–12
55. Peng C, Zhang S, Jewell D, Chen GZ (2008) Progr Natural Sci 18: 777–788
56. Chen WC, Wen TC (2003) J Power Sources 117:273–282
57. Sen P, De A (2010) Electrochimica Acta 55:4677–4684
58. Yang M, Cheng B, Song H, Chen X (2010) Electrochimica Acta 55: 7021–7027
59. Dong B, He BL, Xu CL, Li HL (2007) Materials Science and Engineering B 143:7–13
60. Wang J, Xu Y, Chen X, Sun X (2007) Composites Sci Technol 67: 2981–2985
61. Laforgue A (2011) J Power Sources 196:559–564
62. Frackowiak E, Khomenkob V, Jurewicz K, Lota K, Beguin F (2006) J Power Sources 153:413–418
63. Hou Y, Chen L, Zhang L, Kang J, Fujita T, Jiang J, Chen M (2013) J Power Sources 225:304–310
64. Li X, Zhitomirsky I (2013) J Power Sources 221:49–56
65. Liu H, Wang Y, Gou X, Qi T, Yang J, Ding Y (2013) Materials Science and Engineering B 178:293–298
66. Pasquier AD, Plitz I, Menocal S, Amatucci G (2003) J Power Sources 115:171–178
67. Jang BZ, Liu C, Neff D, Yu Z, Wang MC, Xiong W, Zhamu A (2011) Nano Lett 11:3785–3791
68. Luo JY, Xia YY (2009) J Power Sources 186:224–227
69. Karthikeyan K, Aravindan V, Lee SB, Jang IC, Lim HH, Park GJ, Yoshio M, Lee YS (2010) J Alloys Compounds 504:224–227
70. Hashmil SA, Suematsu S, Naoi K (2004) J Power Sources 137:145–151
71. Zihong S, Anbao YY (2009) Chinese. J Chem Engineering 17(1): 150–155
72. Fuller T, Doyle M, Newman J (1994) J Electrochem Soc 141(1):1–10
73. Verbrugge MW, Koch BJ (1996) J Electrochem Soc 143(2):600–608
74. Gomadam PM, Merritt DR, Scott ER, Schmidt CL, Skarstad PM, Weidner JW (2007) J Power Sources 174(2):872–876
75. Darling R, Newman J (1997) J Electrochem Soc 144(12):4201–4208
76. Levi MD, Aurbach D (1999) Electrochimica Acta 45(1):167–185
77. Despic AR, Drazic DM, Savic-Magic GA, Atanasoski RT (1972) Croat. Chem Acta 44(1):79–87